

www.acsaem.org Article

Polydopamine-Based Polymer Layer for Enhanced Interfacial Properties of Hybrid Ceramic—Polymer Solid Electrolytes

Manuela Ferreira, Robert Schmidt,* Fan Xu, Sanaz Ketabi, Mei Cai, and Yingxi Zhu*



Cite This: https://doi.org/10.1021/acsaem.3c02350



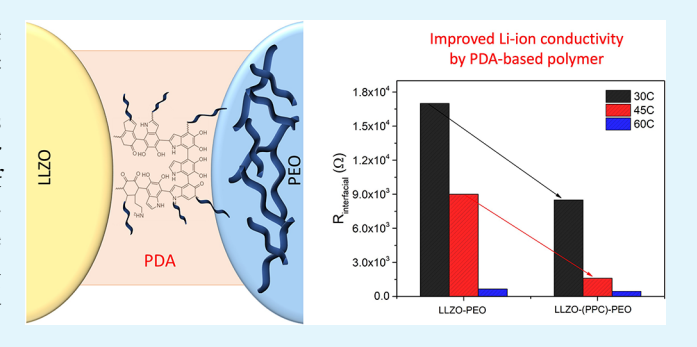
ACCESS I

III Metrics & More

Article Recommendations

s Supporting Information

ABSTRACT: Hybrid ceramic—polymer membranes have emerged as solid-state electrolytes (SSEs) promising high ionic conductivity, strong mechanical strength, and easy processing. However, the inherent incompatibility between inorganic ceramics and organic polymers remains a great challenge for their applications. In this work, we investigated the interaction of polydopamine (PDA)-based polymer with both inorganic garnet-type Li₇La₃Zr₂O₁₂ (LLZO) ceramic and organic poly(ethylene oxide) (PEO) electrolytes to enhance their interfacial binding in both cast membrane from mixed composite slurry and multilayered electrolyte setups. For the LLZO-PEO cast composite membrane, the polymerization of dopamine directly on the LLZO particle



surfaces was explored. PDA-coated LLZO powders can mix well with PEO into a homogeneous composite slurry to considerably improve the processability and smoothness of the resulting cast membrane. For the introduction of PDA-co-PEO polymer as an interfacial layer for the multilayered solid electrolyte setup, substantial improvement in the wettability between the LLZO surface and PEO was observed, suggesting that intimate interfacial contact facilitated by PDA-co-PEO copolymer could be achieved. Most importantly, the introduction of the PDA-based interfacial layer can lead to significant increase of the lithium-ion conductivity to meet the current industrial benchmark of 10^{-4} S cm⁻¹ at room temperature, promising the development of future all-solid-state electrolytes for battery applications.

KEYWORDS: solid electrolyte, interfacial polymer layer, hybrid electrolyte, polymer—ceramic electrolyte, lithium-ion conductivity

1. INTRODUCTION

The increasing interest in safe and sustainable energy storage systems has broadened the studies on lithium-ion batteries (LIBs) now more than ever. 1-4 LIBs are one of the conventional battery systems used in portable electronics, small power tools and appliances, and electric vehicles. However, the flammable organic liquid electrolyte typically used in LIBs has proven to be a reoccurring safety hazard, as well as has limits to achieve higher energy density for future battery demands. 5,6 Recent research on the energy storage field has thereby focused on the development of solid-state electrolytes (SSEs) for LIBs. In contrast to the conventional liquid electrolytes, SSEs can perform at higher safety standards due to the nonflammable properties of their components and also present a wider range of electrochemical stability, which allows for the safe use of batteries with higher energy density.^{7,8} Thus, driven by the search for higher energy density, higher safety, and prolonged life of lithium-ion batteries, SSEs are considered highly as a future electrolyte candidate.9

Some of the most explored types of SSEs are ceramic oxides and polymers. Ceramic oxides include perovskite-type such as Li_{0.33}La_{0.56}TiO₃, LiSICON-type such as Li₁₄Zn(GeO₄)₄, and

garnet-type such as Li₇La₃Zr₂O₁₂ (LLZO). These ceramic materials, especially garnet LLZO, have shown great promises for all solid-state electrolyte fabrication, thanks to their high ionic conductivity and great stability against lithium metal. 15-18 However, ceramic-based SSEs are brittle and exhibit great difficulty in processing, which could result in large interfacial resistance due to their poor contact with the electrodes. 19 Conversely, solid polymer electrolytes, mainly poly(ethylene oxide) (PEO)-based electrolytes, tend to be less challenging in processing and provide great flexibility to achieve intimate contact with the electrodes. However, their low ionic conductivity at room temperature remains a major obstacle to their practical application for LIBs.²⁰ Thus, hybrid ceramic-polymer SSEs that combine their superior properties of both PEO and LLZO have been proposed to overcome their mutual drawbacks. However, the intrinsic incompatibility

Received: September 18, 2023 Revised: October 26, 2023 Accepted: October 30, 2023



ACS Applied Energy Materials

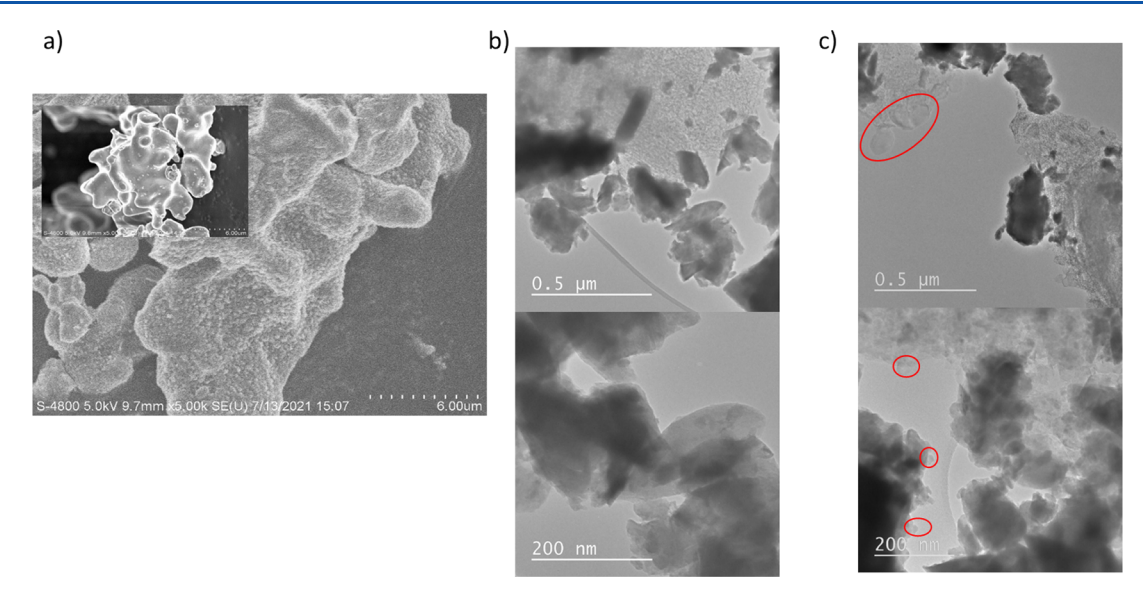


Figure 1. (a) SEM micrograph of HG-LLZO@PDA in contrast to that of plain HG-LLZO (inset) at the same magnification with a scale bar of 6 μ m on each micrograph. TEM images of (b) BM-LLZO and (c) BM-LLZO@PDA shown in two magnifications with the scale bar of 0.5 μ m (top panel) and 200 nm (bottom panel). Highlighted areas as circled indicate the presence of PDA polymer.

between polymer and ceramic materials and resulting poor interfacial contact between them could severely limit the transport of lithium ions due to the increasing interfacial resistance. The distinction in their structure and properties leads to high energy barriers at the surface level that hinder the electrochemical performance. Thus, an additional interfacial layer, which could strongly mediate between ceramic and polymer to enhance their interaction, could be an ideal solution to address the current problem in the development of hybrid ceramic—polymer SSEs.

In this work, we have explored the approach of introducing polydopamine (PDA)-based polymer or copolymer as the interfacial binding material for LLZO and PEO electrolytes to improve the interfacial contact and resulting material properties. PDA is a widely used material for surface modification or functionalization and known for its facile and rapid polymerization process from dopamine monomer. 23,24 The discovery of PDA comes from the study of marine species such as mussels, which are known for secreting adhesive proteins to attach themselves to a variety of ceramic rock surfaces. The proteins secreted from a mussel's foot make use of an oxidative polymerization process of catecholamines to generate biological adhesives suitable for both organic and inorganic substrates. 25,26 Due to the versatility, low cost, and efficacy in its adhesive properties, PDA has been explored as a building block for surface modification in a variety of fields, including the energy storage industry. ^{24,27–32} For instance, PDA has been used to improve the wettability of separators and electrodes, as well as facilitating adequate bonding in carbon-based composites for cathodes. ^{33–36} Given the compatibility of PDA with a variety of materials including some conventional battery-related materials, PDA is investigated in this work to improve the interfacial and electrochemical properties of hybrid inorganic-organic solid-state electrolytes for Li-ion battery application.

Prior research has reported that the conglomeration of LLZO particles in the PEO slurry possesses great challenges to produce homogeneous LLZO-PEO composites, due to the distinct surface energy and resulting in poor wettability between LLZO and PEO.^{37,38} PDA has been used to modify

the interfacial energy on ceramic particles and improve the colloidal dispersion in ceramic-polymer composites, 28,39 yet the study of the effect of PDA interfacial layers on the electrochemical properties of composite high-performing electrolytes has been few. It is noted that prior work on LLZO-PEO electrolytes has mainly focused on adding LLZO as nanofillers to PEO or other solid polymer electrolytes, yet the room-temperature ionic conductivity of such polymerbased solid electrolytes remains below the benchmark of 1 \times 10⁻⁴ S cm⁻¹ as demanded for practical applications. Distinctly, in this work, we have investigated the effect of PDA interfacial layer on the hybrid LLZO-PEO solid-state electrolytes in two different electrolyte configurations, namely, slurry cast membrane and multilayer. While it is much easier to process flexible LLZO-PEO composites in an economic and scalable manufacturing fashion, multilayered electrolytes can provide considerably higher mechanical strength and good dendrite suppression. For the slurry cast membrane, we have grafted dopamine monomers on LLZO particles for in situ polymerization before mixing PDA-grafted LLZO particles with PEO in acetonitrile to make a homogeneous slurry mixture. For the multilayered solid electrolyte setup, we have first conducted the copolymerization of dopamine with amino-functionalized PEO (PDA-co-PEO) and then spin-coated the copolymer on the LLZO pellet surface before the assembly with PEO membrane into a multilayered LLZO-PDA-PEO solid electrolyte.

2. MATERIALS AND METHODS

2.1. Materials. Methoxy polyethylene glycol amine HCl salt of molecular weight (MW) 3000 (PEO3k) was purchased from JenKem Technology USA. PEO of MW 400,000 (PEO400k), lithium bis(trifluoromethanesulfonyl)imide (LiTFSI), high-purity (>98%) methanol and acetonitrile, dopamine hydrochloride, phosphate buffer, and sodium hydroxide (NaOH) solution were purchased from Sigma-Aldrich. PEO and LiTFSI were dried at 50 °C under vacuum for 1–3 days before being used. Methanol and acetonitrile were dried with 20 vol % molecular sieves (3 Å, MS3A4805, Delta Adsorbents) for a minimum of 3 days prior to being used to remove trace moisture. Aluminum-doped LLZO powder, Li_{6.24}La₃Zr₂Al_{0.24}O_{11.98}, was purchased from the NEI Corporation. LLZO pellets were prepared by

hot pressing at 1050 $^{\circ}$ C. The pellets were then cut into slices by using a diamond saw, and the resulting thinner pellets were polished with sandpapers of 2000 grit until completely flat, smooth, and mirror-like surfaces were obtained. The polished LLZO pellets were rinsed with copious amounts of ethanol and acetonitrile and blown dry by nitrogen gas before measurement.

2.2. PDA-*co***-PEO Copolymerization.** The polymerization of dopamine monomers onto various substrates has been widely studied. ^{23,25,27,42} Based on the structural affinity of dopamine with amine-based groups, the copolymerization of dopamine with another amine-containing polymer has been reported previously.⁴³ In this work, an amine-functionalized PEO3k solution of 25 mM was prepared using 0.1 M phosphate buffer for random copolymerization with PDA. The pH of the PEO solution was adjusted to 8.5 using NaOH solution. Dopamine hydrochloride solution was prepared using deionized water (Barnstead Smart2Pure). In a glass vial, PEG3k solutions of varied concentrations, phosphate buffer (0.1 M, pH 8.5), and dopamine solution (10.55 mM) were mixed and gently tumbled overnight at room temperature. The copolymerization reaction stopped after the mixture was turned into a dark brown color, and the final product was purified using ultrafiltration membrane (Microsep Advance Centrifugal Devices with Omega Membrane 3K, Pall Corporation) by continuously centrifuging at 7500g before characterization. After the purification step, the size of the resulting PDA-co-PEG copolymer (PPC) is measured by light scattering (DLS) (ZetaPlus, Brookhaven Instruments). The PPC polymer solution was freeze-dried (Labconco FreeZone 4.5 freeze-dryer) to remove the water content and stored in glovebox before future experimental work.

2.3. Composite LLZO-PEO Electrolyte Preparation. In this work, we prepared the LLZO-PEO composite solid electrolytes using two different ways, one by solution casting membrane from their homogeneous slurry mixture (see Figure 1a,b) and the other by multilayer assembly of a PEO/Li membrane and a PPC copolymer-coated LLZO pellet.

PDA-grafted LLZO particles (LLZO@PDA) via in situ dopamine polymerization were prepared by dispersing ball-milled LLZO powder in methanol solution, adding dopamine hydrochloride of 2 mg/mL and mixing overnight. The products of PDA-coated LLZO particles were removed from the solution, washed with methanol copiously, and dried in a vacuum oven overnight at 40 °C.

For membrane casting, LLZO or LLZO@PDA powder was first suspended in acetonitrile by sonication for 10 min at a concentration of 7.5, 15, and 30 wt % relative to acetonitrile and subsequently added with LiTFSI at a concentration of 0.274 M. Finally, PEO400k was slowly added at the fixed ether-oxygen-to-lithium molar ratio, EO:Li+ = 8:1, and the mixture was constantly stirred overnight at 30 °C to obtain homogeneous composite slurry. The slurry was then cast on a clean and flat PTFE board, using a doctor blade to drag the slurry across the board surface for a uniform film. The cast membranes were placed under vacuum for 1-2 days until it became completely dry. Finally, the composite films were peeled-off and labeled as "LLZO-PEO" or "LLZO@PDA-PEO" corresponding to the films without or with PDA additives, respectively, and stored in an argon-filled glovebox before experimental characterization. PEO/Li membranes as a control were also prepared with the same EO⁻:Li⁺ = 8:1 in a similar manner yet without the LLZO addition.

For the multilayer solid electrolyte assembly, the LLZO pellet was gold-sputtered on the opposite side for electrochemical characterization before PPC coating. PPC copolymer in its acetonitrile solution of 0.12 g/mL was spin-coated onto a polished LLZO pellet first for 30 s at a speed of 2000 rpm, as a coating step, and then for another 30 s at 5000 rpm as a drying step. After drying the PPC-coated LLZO pellet under vacuum overnight at room temperature, a PEO/Li membrane with similar diameter was placed on top of it and pressed together into a coin cell. The multilayered membranes were annealed at 45 °C for 1–3 h and cooled to room temperature before further measurements. The multilayered SSEs were labeled as "LLZO–PPC-PEO/Li" and "LLZO-PEO/Li" corresponding to the ones with and without a PPC copolymer coating on LLZO pellets, respectively.

2.4. Characterization. Morphological structures of the LLZO powder and pellet surfaces were characterized by scanning electron microscopy (SEM, Hitachi field emission SEM S4800) and transmission electron microscopy (TEM, aberration-corrected JEOL JEM-2100F). For SEM characterization, the LLZO pellet was sputter-coated with a thin gold layer of approximately 10 nm thick. For TEM characterization, the as-synthesized LLZO powder samples were prepared by grinding the powder between two clean glass slides and then dusting the ground fine powder onto lacy-carbon-coated Cu TEM grids.

The wettability of PEO on untreated and PPC copolymer-coated LLZO pellet surfaces was determined by a sessile droplet goniometer (Ramehart, 250-F1) with PEO400k solution of 5 wt % in acetonitrile. The contact angle of PEO droplets on untreated and PPC-coated LLZO pellets was measured at three different spots and averaged to be reported in this work.

The thermal properties of PDA-coated and uncoated LLZO nanoparticles were studied by thermogravimetric analysis (TGA) under an argon environment from room temperature to 600 °C at a heating rate of 10 °C/min. After heating to 600 °C, the sample was held at 600 °C under purged dry air to remove any residual polymer.

Electrochemical impedance spectroscopy (EIS) was performed with a potentiostat (Biologic SP-200) to determine the lithium-ion conductivity in different LLZO-PEO electrolyte setups. In all the measurements, the testing composite solid electrolyte was sandwiched between two stainless steel plates and placed inside a coin cell, which was sealed in an argon-filled glovebox. The EIS experiment was carried over a frequency range from 100 mHz to 7 MHz at a constant applied peak-to-peak voltage of 10 mV. The EIS measurements were taken at every 5 °C temperature increasing from 25 to 60 °C, with at least 30 min to reach thermal equilibrium between any two successive measurements. In potentiostatic conditions, the EIS technique was used to measure the impedance of a system, by detecting the current responses to small-amplitude sinusoidal applied voltage at an angular frequency, ω . 44,45 The measured impedance, Z, can be described by $Z(\omega) = Z_0 \cos(\varphi) + jZ_0 \sin(\varphi) = Z' + jZ''$ (eq 1), which is derived elsewhere, where $j = \sqrt{-1}$ is the imaginary unit, $\omega = 2\pi f$ is the angular frequency, f is the frequency, and ϕ is the phase angle shift between the voltage and current. The Nyquist plot is typically used to represent the collected impedance data, where the real component is on the x-axis (Z') and the negative complex component of the impedance is on the y-axis (-Z''). To interpret and analyze the resulting Nyquist plot, the resulting spectra are fitted with a model from an equivalent circuit (see the Supporting Information). The conductivity of the electrolytes can be calculated using $\sigma = L/RS$ (eq 2), where L is the thickness, S is the area of the electrolyte, and R is the measured bulk resistivity from the fitting of the Nyquist plot.

Linear sweep voltammetry (LSV) was used to measure the electrochemical stability of the hybrid electrolytes using a Biologic SP-200. The LSV test was performed at a sweep rate of 1 mV/s from 2 to 5 V (vs Li/Li^+) where lithium metal was used as the counter and reference electrode and stainless steel was the working electrode.

3. RESULTS AND DISCUSSION

3.1. Coating of PDA Polymer on LLZO Surface. The polymerization of dopamine onto LLZO powders was performed with both hand-ground LLZO and ball-milled LLZO, referred to as HG-LLZO and BM-LLZO, respectively. SEM images of the HG-LLZO of 5 to 20 μ m in size after the PDA surface modification confirm the complete coverage of the ceramic particles by PDA, as observed in Figure 1a, in clear contrast to the uncoated particles depicted in the inset of Figure 1a. However, due to the need for nanometer-scale and uniform size distribution of LLZO particles, the LLZO powder is commonly ball-milled and dried prior to use. The average LLZO particle size after ball-milling is 100-200 nm, which is acceptable and optimum for composite membrane casting. The highlighted areas on TEM micrographs shown in Figure

ACS Applied Energy Materials

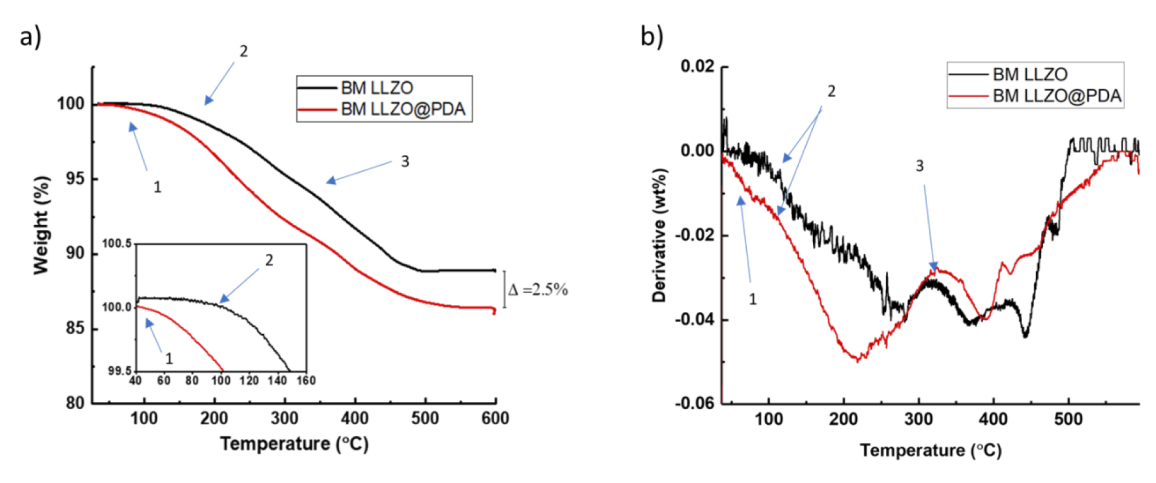


Figure 2. TGA profiles of (a) LLZO (black) and LLZO@PDA (red) and (b) their respective derivatives. Inset of panel (a): Blow-out of the low temperature region, where the mass loss of PDA is observed. Mass change 1 is identified as the PDA mass loss initiation, peak 2 is LiOH decomposition, and peak 3 is the decomposition of Li₂CO₃.

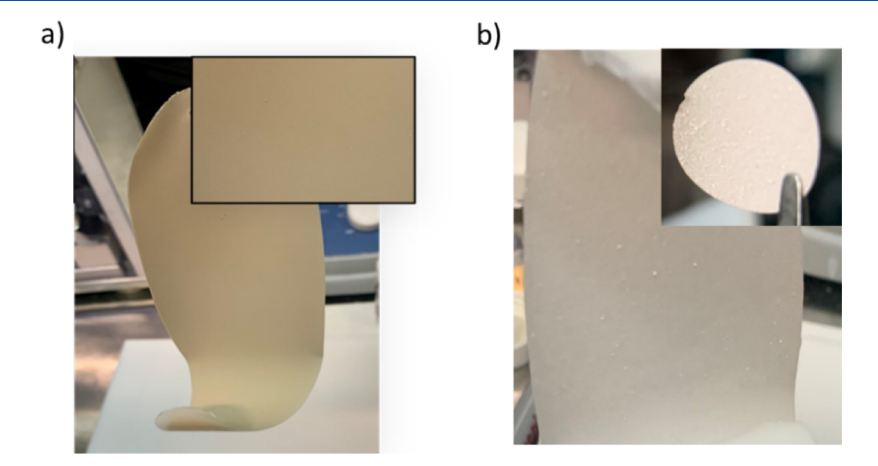


Figure 3. Digital photographs of composite electrolyte membranes prepared with (a) LLZO@PDA and (b) LLZO added in PEO acetonitrile solution. Inset: Blow-out of the morphological view of corresponding cast membranes.

1b,c also indicate the polymeric materials as the only noncrystalline structure spotted on the micrographs. Additionally, the structure in these areas appears distinct from that of other passivation materials on LLZO such as Li₂CO₃ or LiOH. Although elemental mapping by energy-dispersive X-ray spectroscopy with TEM could provide direct evidence of PDA coating on LLZO surface, combined SEM and TEM results, as well as the measured change of thermal properties and wettability of LLZO with PDA coating (see Figures 2 and 6 below, respectively), confirm the effective coating of polymerized PDA layer on LLZO surface.

To further verify the grafting of PDA polymers on LLZO surface, TGA characterization was performed with BM-LLZO particles as the temperature-dependent weight loss profile is shown in Figure 2a in comparison to that of pristine BM-LLZO. The derivative of the measured TGA profile is also compared in Figure 2b to help identify the temperature range for the weight loss of distinct components in the samples. The first mass loss, labeled as "1" and identified only in the red curve for the PDA-coated sample, occurs at lower temperatures than that for the second mass loss as labeled in "2" (see the inset), which indicates the decomposition of PDA at $T = \sim 20-50$ °C. The second mass loss was observed in both samples and is consistent with the reported mass loss from LiOH, which is well expected to occur at $T \sim 200$ °C based on

previous TGA-MS work.⁴⁸ A third mass loss is observed to commence at $T = \sim 400$ °C, which is attributed to the loss of both H₂O and CO₂. Above this temperature range, it is expected that Li₂CO₃ decomposes from the surface with the lithium ion reinserting into the LLZO structure to displace hydrogen ion while hydrogen combining with the remaining carbonate to form H₂O and CO₂.⁴⁸ Overall, the TGA results note a 2.5% mass difference at 600 °C when comparing PDA-coated LLZO to plain LLZO, which is consistent with the combined mass of the PDA and associated impurities (proton exchange, etc.).

3.2. Effect of Interfacial PDA Layer on Cast Composite Electrolyte. Both SEM and TGA results above confirmed that PDA can be firmly grafted onto LLZO ceramic powders. Next, we studied the effect of PDA coating on the bulk-scale membrane morphology and homogeneity of the cast LLZO-PEO solid electrolyte membranes from their mixture slurry to ensure the feasibility of subsequent electrochemical measurements. It appears that the slurry of the LLZO@PDA and PEO mixture in acetonitrile is homogeneous without any noticeable agglomeration of LLZO in contrast to the observed aggregation and sedimentation of plain LLZO powder in its mixed slurries with PEO, suggesting the improved dispersion of LLZO@PDA in the mixture. Also as shown in Figure 3a, the cast membrane from LLZO@PDA—PEO slurry containing 15

ACS Applied Energy Materials

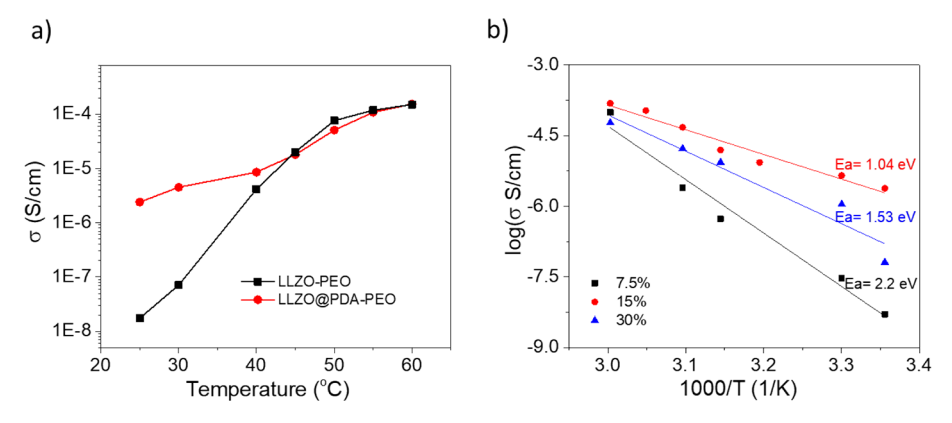


Figure 4. (a) T-dependent bulk lithium-ion conductivity, σ , of uncoated LLZO-PEO (black squares) and LLZO@PDA-PEO (red circles) added to PEO composite membranes. (b) Arrhenius plot of σ against 1000/T of LLZO@PDA-PEO composite membranes containing 7.5 wt % (black squares), 15 wt % (red circles), and 30 wt % (blue triangles) LLZO@PDA in their mixture with PEO400k.

wt % of LLZO@PDA appears smooth without any visible grainy aggregates, in contrast to the coarse membrane formed from plain LLZO-PEO mixture as shown in Figure 3b. The dispersion of LLZO@PDA nanoparticles throughout the composite suggests the promising benefits on processing the ceramic—polymer composite electrolyte membrane with high flexibility and homogeneity.

The cast LLZO@PDA-PEO membrane of 90 \pm 5 μ m in thickness and 13.5 mm in diameter confined in a symmetrical stainless steel coin cell was examined for its electrochemical performance. The Nyquist plots from the EIS impedance measurements at different temperatures (T) based on eq 1 are shown in Figure S1. The Nyquist plots display a typical semicircle at high frequency, corresponding to the bulk resistance of the solid electrolyte, and a low-frequency tail resulting from the behavior of using ion blocking stainless steel electrodes. The bulk resistance, R_{bulk} , of the solid electrolyte can be obtained by fitting the Nyquist plot using the equivalent circuit as displayed in Figure S1b. Accordingly, the ionic conductivity, σ , against varied T is obtained using eq 2 and plotted in Figure 4a, given the measured L = 0.009 cm and S =1.43 cm² of the overall testing cell whose dimension is nearly independent of T. In the control experiment, we also determined the ionic conductivity of cast plain LLZO-PEO membrane under the same conditions as the LLZO@PDA-PEO as compared in Figure 4a. Clearly, we observed a drastic improvement in the ionic conductivity by more than 2 orders of magnitude at T = 25-30 °C for LLZO@PDA-PEO electrolytes compared to that of LLZO-PEO electrolytes without PDA. The effect of PDA interfacial coating on enhancing ionic conductivity in composite membranes diminishes when T exceeds 45 °C upon approaching its melting temperature around 60 °C at which the high conductivity of liquid-like PEO electrolyte is well expected. 49,50 Nevertheless, the improved σ at the low T = 25-45 °C of LLZO@PDA-PEO electrolytes suggests the effectiveness of the PDA coating to minimize the interfacial incompatibility between LLZO and PEO and thereby improve the overall electrochemical performance of the cast composite solid electrolyte.

To determine the optimal formulation of LLZO@PDA–PEO composites to achieve superior ionic conductivity, we investigated the effect of LLZO@PDA concentration in the composite electrolyte on σ . Figure 4b depicts the Arrhenius plots of the measured σ against 1/T for membranes with varied

LLZO@PDA weight fraction. The conductivity of all dried composite membranes follows the same trend over the measured temperature range, and the ionic conductivity, σ , ranges from 5.1×10^{-9} to 1.6×10^{-4} S cm⁻¹ over the temperature range of T = 30-60 °C, in good agreement with the previously reported σ of other hybrid composites using mixtures of PEO and LLZO.⁵¹ The σ at T = 60 °C for all LLZO@PDA-PEO solid electrolytes satisfies the standard criteria of $\sigma \geq 10^{-4} \text{ S cm}^{-1}$ suitable for Li-ion battery application. Moreover, the highest σ is found for the membranes with 15 wt % LLZO@PDA, followed by 30 wt % and the lowest with 7.5 wt % LLZO@PDA. Furthermore, all the data for each membrane can be well fitted linearly to yield the activation energy, E_a by following $\sigma = Ae^{-E_a/\kappa T}$, where A and κ are the pre-exponential factor and Boltzmann constant, respectively. The composite membrane with 15 wt % LLZO@ PDA exhibits the lowest measured E_a of 1.04 eV in comparison to $E_a = 1.53$ and 2.2 eV for the cases of 30 and 7.5 wt % LLZO@PDA, respectively, indicating an optimal LLZO@PDA content of ~15 wt % with PEO 400k to achieve the highest ion transport. The observed presence of optimal LLZO@PDA concentration in the composite electrolytes with PEO agrees with previous reports on tantalum (Ta)-doped LLZO-PEO composite electrolytes,⁵² which attributes the added Ta to facilitate the Li+ transfer pathways with a certain optimal microstructure. We expect that in a similar fashion, the concentration and distribution of LLZO@PDA could either lead the Li⁺ transfer pathway through the PEO chains or through the interconnected LLZO particles and thereby affect the overall effectiveness of the electrolyte,⁵² yet the detailed transport mechanism warrants future studies. We recognize that despite improved room-temperature ionic conductivity, the σ of the LLZO@PDA-PEO400k composite membrane remains to underperform for industrial standards; a comprehensive study of the LLZO-PDA-PEO interfacial interaction as well as optimal formula including PEO Mw is highly desired for future development of composite film-type solid electro-

3.3. Effect of the Interfacial PPC Layer on Multilayered Solid Electrolyte. To further verify the effect of the PDA interfacial layer to improve the interfacial compatibility between LLZO and PEO solid electrolytes, we also examined the ionic conductivity of the multilayered LLZO—PDA-PEO electrolyte configuration. Specifically, in this configuration, we explored the PPC copolymer, instead of PDA homopolymer,

as the interfacial coating and explored its effect on the electrochemical properties of the multilayered inorganicorganic solid electrolytes. The addition of short PEO chains as blocks to copolymerize with dopamine is expected to further improve LLZO-PEO compatibility in hybrid organicinorganic solid electrolytes with the following considerations. The PPC copolymer is very stable and allows tunable parameters regarding each block chain length to tune and optimize the interfacial structure and the resulting electrochemical properties. The incorporation of PEO blocks into the interfacial polymer layer is expected to further enhance the interfacial interaction with the PEO layer in the multilayered electrolytes. Also, as the synthesis of PPC is conducted independently, there is no need to submerge the LLZO particles or pellets in any solvent over an extensive time period, as is needed for the polymerization of dopamine grafted on LLZO particles. This independent synthesis method minimizes the undesired formation of passivation layers containing LiOH and Li₂CO₃ on the moisture-sensitive surface of the LLZO material.5

For the random copolymerization of PPC investigated in this work, we have mainly used the amino-functionalized PEO3k added to the dopamine solution of a fixed 2.0 mg/mL concentration. After reaction overnight, the clear solution becomes dark brown in color as exhibited in the inset of Figure 5, indicating the successful polymerization of dopamine.²³ The

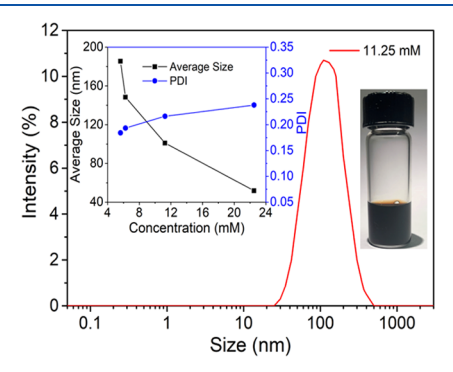


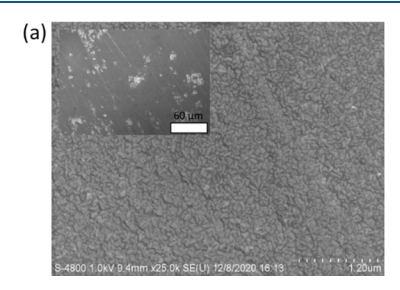
Figure 5. DLS intensity-size profile of the synthesized PDA–PEO copolymer. Inset: (left) Measured copolymer size (black squares) and PDI (blue circles) against PEO concentration are plotted in left and right *y*-coordinate axis, respectively; (right) digital photograph of the solution shown in dark brown color, indicating the completion of the PDA–PEO copolymerization.

size and size distribution of PPC with varied PEO concentrations and reaction times were determined by DLS after purification. The PPC synthesized with added PEO3k of 11.25 mM in concentration exhibited an average size of

approximately 102 nm with desired narrow size distribution of polydispersity, PDI = 0.215, shown in Figure 5. The size of the synthesized PPC was found to decrease from 185 to 52 nm with increasing PEO concentration from 5 to 22.5 mM, as detailed in the inset of Figure 5, suggesting the dependence of the average size of PPC copolymers on the availability of the amino-functionalized PEO for the reaction. It is noted that the PDI remained below 0.24 for all the varied PEO concentrations, suggesting the relatively narrow size distribution of PDA blocks in the copolymers.

To examine the interaction of PPC with both LLZO and PEO, we have characterized the morphological structure of PPC coating on LLZO as well as the wettability of PEO liquid on the PPC-coated LLZO surface. The microstructure of spincoated PPC layer on a polished LLZO pellet surface was characterized by SEM. The SEM micrograph in Figure 6a clearly exhibits complete and homogeneous coverage of PPC copolymer coating on LLZO surface in contrast to featureless smooth untreated surface (see the inset of Figure 6a), confirming strong affinity of PPC on LLZO surface. It should be noted that SEM micrographs also indicate nonuniform thickness of the PPC coating as the PPC layer could be formed by PPC blob/spheroid aggregates of $\leq 1 \mu m$ in size that merge into an approximately continuous layer. Thus, it is challenging to exactly quantify the coating thickness, as the thickness measurement by either ellipsometry or AFM was unsuccessful. Instead, we have examined the modification of LLZO surface energy by the PPC coating by the contact angle measurement of PEO400k droplet of 5 wt % concentration in acetonitrile solution. As the sessile droplet profiles are compared in Figure 6b,c, the contact angle of PEO droplet on PPC-coated LLZO surface is $21 \pm 2.5^{\circ}$ in comparison that of $73 \pm 3.7^{\circ}$ measured on the bare untreated surface, clearly indicating the effective modification of LLZO surface chemistry by the adsorbed PPC layer.^{38,54} We also observed that the low contact angle remained nearly unchanged over several hours, suggesting the dense and robust coating of PPC on the LLZO surface. The enhanced wettability of PEO on PPC-coated LLZO in comparison to its poor wetting on the pristine LLZO surface also confirmed the strong interaction of PPC copolymer with both LLZO and PEO.

To understand the relationship between LLZO-PEO interfacial interaction and electrochemical properties, we also examined the lithium-ion transport of the multilayered LLZO-PPC-PEO solid electrolyte in comparison to the cases of plain LLZO pellet, PEO/Li electrolyte, and bilayered LLZO-PEO/Li solid electrolytes. The Nyquist plots of the plain LLZO pellet at varied $T=30-60\,^{\circ}\mathrm{C}$ are exhibited in Figure S2a and analyzed in the similar fashion as the cast composite electrolytes discussed in section 3.2. For the control



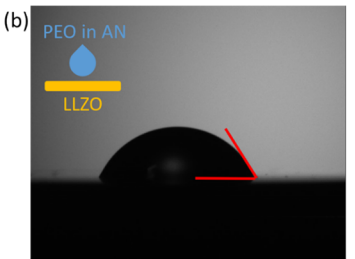




Figure 6. (a) SEM micrograph of the morphological structure of the PDA-co-PEO coating layer on a polished LLZO pellet. Photographs of the sessile droplet of 5 wt % PEO solution in acetonitrile on (b) untreated LLZO in contrast to (c) PDA-co-PEO-coated LLZO surface.

of the plain LLZO pellet, we obtained $\sigma = 3.0 \times 10^{-4} \text{ S cm}^{-1}$ given the measured L = 0.08 cm and S = 1.327 cm² at 30 °C with the testing coin cell. As shown in Figure S2c, the logarithmic plot of σ against 1000/T can be fitted linearly by the Arrhenius' equation to obtain the activation energy, E_a , for lithium-ion transport in LLZO, $E_a = 0.41$ eV, which is in good agreement with the previously reported activation energy of 0.32-0.41 eV for plain LLZO. ⁵⁵⁻⁶⁰ In this work, we have also compared the performance among three other cases, PEO/Li membrane, LLZO-PEO/Li bilayer membrane, and LLZO-PPC-PEO/Li multilayer membrane, with corresponding Nyquist plots exhibited in Figure S3. These membranes exhibited features in the Nyquist plots corresponding to different components of varied electrochemical properties in the testing cell, namely LLZO, PEO, and PPC. Each of the cells exhibited one defined semicircle at high frequency, representing the bulk resistance of the assembly. Additionally, for the bilayer and multilayer solid electrolytes, the spectra at lower frequencies depicted the formation of a partial second semicircle mixed with the tail. The second semicircle profile represents the interfacial resistance that arises from the different layers on the cell set up, for instance, the resistance from PEO/Li membrane and PPC interfacial layer with the LLZO pellet in the multilayer electrolyte. We fitted the spectra by using the circuit model depicted in Figure S4b to obtain the bulk resistance, R_{bulk} , and thereby calculated the σ of the entire multilayered LLZO-PPC-PEO electrolyte, σ , with $R_{\text{bulk}} = 250$ Ω using eq 2, where L = 0.0851 cm and S = 1.327 cm² for the entirely assembled coin cell setup in this work. It is noted that due to the complexity and model-based analysis to determine the interfacial ion conduction, we merely focused on the overall bulk σ , not the interfacial resistance across the PPC layer that warrants future study. Nevertheless, it is evident as summarized in Table 1 that the obtained R_{bulk} exhibits the

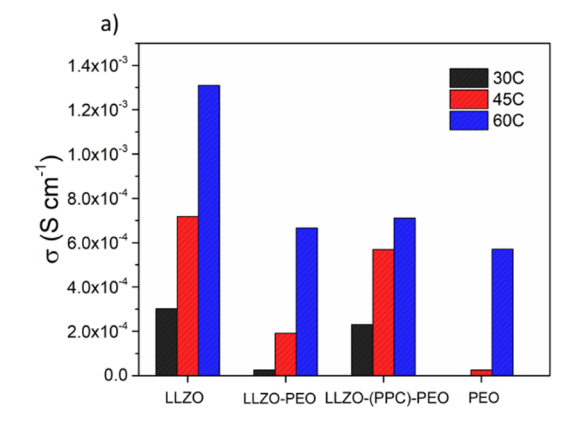
Table 1. Summary of $R_{\rm bulk}$ and σ for the Solid Electrolytes in Varied Configurations at 30°C

| solid electrolyte | thickness (cm) | $R_{\mathrm{bulk}}\left(\Omega\right)$ | σ (S cm ⁻¹) |
|-------------------|----------------|--|--------------------------------|
| LLZO | 0.08 | 200 | 3.02×10^{-4} |
| LLZO-PPC-PEO | 0.0851 | 277 | 2.31×10^{-4} |
| LLZO-PEO | 0.085 | 2,550 | 2.51×10^{-5} |
| PEO | 0.005 | 9,382 | 4.02×10^{-7} |

following trend at T=30 °C: LLZO \cong LLZO-PPC-PEO/Li < LLZO-PEO/Li < PEO/Li. It is important to observe the reduction in the $R_{\rm bulk}$ for Li-ion transport in the LLZO-PPC-PEO/Li multilayer membrane from that of the LLZO-PEO bilayer one, suggesting the effectiveness of the PPC interfacial layer on improving interfacial contact between LLZO and PEO and thereby improving the ionic conductivity of the composite solid electrolytes.

As the room-temperature ionic conductivity is considered as a critical electrochemical property in evaluating the industrial applicability of SSEs, we have examined the trend of the impedance of different SSEs at T = 30-60 °C. As compared in Figure 7a, the LLZO pellet among four different electrolyte setups in this work exhibits the highest σ at each of the measurement temperatures, that is, $\sigma = 3.02 \times 10^{-4} \text{ S cm}^{-1}$ at 30 °C, while PEO/Li exhibits the worst $\sigma = 10^{-7} \text{ S cm}^{-1}$ at 30 °C, which is decreased over 3 orders of magnitude from 10⁻⁴ S cm⁻¹ at 60 °C. Yet, it is most interesting to compare the cases between LLZO-PEO/Li and LLZO-PPC-PEO/Li multilayer electrolytes. The introduction of PPC interfacial layer led to the increase of σ by 1 order of magnitude to $\sigma = 2.3 \times 10^{-4}$ S cm⁻¹ for LLZO-PPC-PEO/Li from $\sigma = 2.6 \times 10^{-5} \text{ S cm}^{-1}$ for LLZO-PEO/Li membrane without PPC at the same T = 30°C, approaching the value of the LLZO pellet. Such PPCinduced improvement in σ is also confirmed at all the varied temperatures up to 60 °C.

The introduction of the interfacial PPC coating can effectively reduce the interfacial resistance to address the incompatibility between the ceramic and the polymer solid electrolytes. It should be noted that the interfacial impedance for the multilayered electrolytes can be a reflection on the efficacy of the added coating with optimal copolymer content, interfacial thickness, and structure. As this work is focused on the fundamental feasibility of PDA-based polymer coating to enhance the interaction between LLZO and PEO, we merely examined the effect of the PDA-based interfacial layer on the ionic conductivity of LLZO-PEO composite electrolytes without conducting a comprehensive battery performance test, which warrants a future study. As the thickness of the PPC coating was thinner than 1 μ m and can be negligible in comparison to that of LLZO pellets (of $\sim 800 \mu m$) and PEO/ Li membranes (of $\sim 50 \mu m$), we can compare the impedance spectra of LLZO-PEO/Li and LLZO-PPC-PEO/Li by neglecting the contribution of PPC conductance to the overall



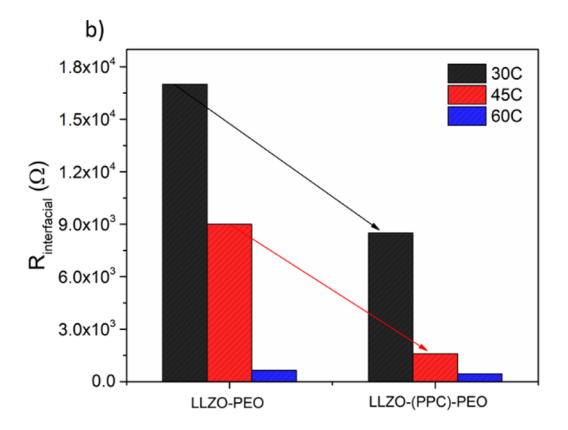


Figure 7. (a) Calculated bulk lithium-ion conductivity, σ, of different multilayered solid electrolytes, LLZO–PPC-PEO, and LLZO-PEO in comparison to two control solid electrolytes of LLZO and PEO/Li membranes at varied temperatures of 30 °C (black column), 45 °C (red column), and 60 °C (blue column). (b) Interfacial impedance, R_{interfacial} of the LLZO-PEO and LLZO-(PPC)-PEO multilayered electrolytes.

bulk resistance. The second semicircles in the intermediate frequency range of LLZO-PEO/Li and LLZO-PPC-PEO/Li (as indicated in Figure S4) could be used to obtain the interfacial resistance, $R_{\text{interfacial}}$. Hence, we examined the Tdependent R_{interfacial} of the multilayered electrolyte with and without the PPC interfacial thin layer to further quantify its effectiveness on the ceramic-polymer solid electrolytes as shown in Figure 7b. At both T = 30 and 45 °C, a significant reduction of nearly 50% in the measured $R_{\text{interfacial}}$ was observed with LLZO-PPC-PEO/Li in comparison to that of LLZO-PEO/Li. At elevated T = 60 °C, the difference in $R_{\text{interfacial}}$ appeared negligible for which we attributed to increased ion mobility at high temperature, where both PEO and PDA-co-PEO could undergo a transition from semicrystalline to amorphous phase as indicated by their T-dependent thermal stability (as shown in Figure S5). Given that the main challenge of polymer-based solid electrolytes is centered on the poor ionic conductivity at low T (below 60 °C), it is of great promise that the addition of a PPC layer can indeed reduce the interfacial impedance at low T to make a hybrid ceramicpolymer solid electrolyte practical for Li-ion battery applications.

For a battery with this multilayered setup of hybrid inorganic-organic solid electrolyte, a combination of three factors needs to be considered: ionic conductivity, chemical stability, and scalable manufacturability at reasonable cost without significant contamination. While the choice of battery active materials is outside the scope of this work, this study has confirmed that a battery could be made from such composite solid electrolyte materials while satisfying each of these criteria. For reference, typical lithium-ion batteries with a liquid electrolyte and separator have conductivity $\sim 10^{-3}$ to 10^{-4} S cm⁻¹ across the polymer separator, based on a MacMullen number of 10.⁶¹ The conductivity of the composite solid electrolyte in this study is sufficiently close to that of the traditional liquid electrolyte to make a reasonable alternative to the traditional setup. Another solid electrolyte, LIPON, has been successfully commercialized, with even lower conductivity of $\sim 10^{-6}$ S cm⁻¹, by minimizing the thickness of the film to keep resistances reasonable. 62-64 Our data obtained by linear sweep voltammetry also support their use with cathode materials to >4.5 V (see Figure S6), confirming composite stability against lithium metal. Finally, the cost and thickness of a solid-state electrolyte need to be considered, with a cost target of \sim \$7 m⁻² considered reasonable⁶⁵ and a target of \sim 20 μ m or less is typically regarded as required to minimize both resistance and cost. 66 Hence, future work could be continued to optimize such interfacial polymer layers to enable scalable manufacturing of composite ceramic-polymer solid electrolytes with improved electrochemical performance against a variety of electrodes.

4. CONCLUSIONS

This study addressed the challenge of high interfacial impedance in current hybrid ceramic—polymer solid electrolytes by introducing a strongly adsorbed polymer interfacial layer. We have explored a new approach to developing hybrid organic—inorganic solid electrolytes by introducing PDA-based polymer or copolymer layers at the LLZO-PEO interfaces on both multilayered setup and cast membrane from composite mixture slurry for lithium-ion battery application. To the best of our knowledge, this is the first time that such a polymer interfacial layer is investigated to improve the interaction and

ionic conductivity of hybrid ceramic—polymer solid electrolytes. For both setups, we have experimentally demonstrated that the PDA-based interfacial layer can effectively enhance the interaction between incompatible LLZO and PEO electrolytes with a resulting improvement in their interfacial wettability and contact. Most importantly, with the introduction of the PDA-based interfacial polymer layer to the LLZO-PEO system, we have observed a significant reduction of $\sim\!50\%$ in the interfacial impedance and the elevation of the overall ionic conductivity to approach 10^{-4} S cm $^{-1}$ at room temperature (20–50 °C) to meet the current benchmark for practical lithium-ion battery application.

In perspective, both setups of hybrid solid electrolytes in this study provide that a battery could be produced under the ionic conductivity that is not adversely impacted and using the materials that have been processed and tested in a scalable manner while contaminant phases are controlled. Hence, this study supports the benefits of modifying the interfaces of ceramic—polymer solid electrolytes with an interfacial PDA-containing polymer layer, paving a promising pathway to enhance their interfacial contact and electrochemical performance of inorganic—organic hybrid solid electrolytes.

ASSOCIATED CONTENT

Supporting Information

The Supporting Information is available free of charge at https://pubs.acs.org/doi/10.1021/acsaem.3c02350.

Additional experimental results, including Nyquist plots, DCS, and LSV profiles of different control samples (PDF)

AUTHOR INFORMATION

Corresponding Authors

Robert Schmidt — General Motors Global Research and Development Center, Warren, Michigan 48090, United States; Email: Robert.d.schmidt@gm.com

Yingxi Zhu — Department of Chemical Engineering and Materials Science, Wayne State University, Detroit, Michigan 48202, United States; ⊚ orcid.org/0000-0002-7968-1640; Email: yzhu3@wayne.edu

Authors

Manuela Ferreira — Department of Chemical Engineering and Materials Science, Wayne State University, Detroit, Michigan 48202, United States; orcid.org/0000-0001-8795-7179

Fan Xu – General Motors Global Research and Development Center, Warren, Michigan 48090, United States

Sanaz Ketabi — General Motors Global Research and Development Center, Warren, Michigan 48090, United States Mei Cai — General Motors Global Research and Development Center, Warren, Michigan 48090, United States; orcid.org/0000-0001-8631-8471

Complete contact information is available at: https://pubs.acs.org/10.1021/acsaem.3c02350

Author Contributions

All authors listed have made a substantial, direct and intellectual contribution to the work, and approved it for publication.

Funding

M.F. and Y.Z. are grateful for the financial support from the National Science Foundation (NSF CMMI-1914436).

Notes

The authors declare no competing financial interest.

REFERENCES

- (1) Wang, Q.; Zhang, G.; Li, Y.; Hong, Z.; Wang, D.; Shi, S. Application of phase-field method in rechargeable batteries. *npj Computational Materials* **2020**, *6* (1), 176.
- (2) Qu, J.; Ning, C.; Feng, X.; Yao, B.; Liu, B.; Lu, Z.; Wang, T.; Seh, Z. W.; Shi, S.; Zhang, Q. Identifying Hidden Li–Si–O Phases for Lithium-Ion Batteries via First-Principle Thermodynamic Calculations. *Energy & Environmental Materials* **2022**, *5* (3), 865–871.
- (3) Kim, T.; Song, W.; Son, D.-Y.; Ono, L. K.; Qi, Y. Lithium-ion batteries: outlook on present, future, and hybridized technologies. *Journal of Materials Chemistry A* **2019**, 7 (7), 2942–2964.
- (4) Wu, F.; Maier, J.; Yu, Y. Guidelines and trends for next-generation rechargeable lithium and lithium-ion batteries. *Chem. Soc. Rev.* **2020**, 49 (5), 1569–1614.
- (5) Kong, L.; Li, C.; Jiang, J.; Pecht, M. G. Li-Ion Battery Fire Hazards and Safety Strategies. *Energies* **2018**, *11* (9), 2191.
- (6) Sun, Y.-K. Promising All-Solid-State Batteries for Future Electric Vehicles. ACS Energy Letters 2020, 5 (10), 3221–3223.
- (7) Zhang, Z.; Shao, Y.; Lotsch, B.; Hu, Y.-S.; Li, H.; Janek, J.; Nazar, L. F.; Nan, C.-W.; Maier, J.; Armand, M.; Chen, L. New horizons for inorganic solid state ion conductors. *Energy Environ. Sci.* **2018**, *11* (8), 1945–1976.
- (8) Zhu, Y.; He, X.; Mo, Y. First principles study on electrochemical and chemical stability of solid electrolyte—electrode interfaces in all-solid-state Li-ion batteries. *Journal of Materials Chemistry A* **2016**, 4 (9), 3253–3266.
- (9) Armand, M.; Tarascon, J. M. Building better batteries. *Nature* **2008**, 451 (7179), 652–657.
- (10) Kwon, W. J.; Kim, H.; Jung, K.-N.; Cho, W.; Kim, S. H.; Lee, J.-W.; Park, M.-S. Enhanced Li+ conduction in perovskite Li3xLa2/3−x□1/3−2xTiO3 solid-electrolytes via microstructural engineering. *Journal of Materials Chemistry A* **2017**, *5* (13), 6257−6262.
- (11) Wu, J.-F.; Chen, E.-Y.; Yu, Y.; Liu, L.; Wu, Y.; Pang, W. K.; Peterson, V. K.; Guo, X. Gallium-Doped Li7La3Zr2O12 Garnet-Type Electrolytes with High Lithium-Ion Conductivity. ACS Appl. Mater. Interfaces 2017, 9 (2), 1542–1552.
- (12) Wang, Q.; Wu, J.-F.; Lu, Z.; Ciucci, F.; Pang, W. K.; Guo, X. A New Lithium-Ion Conductor LiTaSiO5: Theoretical Prediction, Materials Synthesis, and Ionic Conductivity. *Adv. Funct. Mater.* **2019**, *29* (37), 1904232.
- (13) Wu, J.-F.; Zou, Z.; Pu, B.; Ladenstein, L.; Lin, S.; Xie, W.; Li, S.; He, B.; Fan, Y.; Pang, W. K.; Wilkening, H. M. R.; Guo, X.; Xu, C.; Zhang, T.; Shi, S.; Liu, J. Liquid-Like Li-Ion Conduction in Oxides Enabling Anomalously Stable Charge Transport across the Li/ Electrolyte Interface in All-Solid-State Batteries. *Adv. Mater.* **2023**, 35 (40), 2303730.
- (14) Guo, Q.; Xu, F.; Shen, L.; Deng, S.; Wang, Z.; Li, M.; Yao, X. 20 μ m-Thick Li6.4La3Zr1.4Ta0.6O12-Based Flexible Solid Electrolytes for All-Solid-State Lithium Batteries. *Energy Mater. Adv.* **2022**, 2022, 9753506 DOI: 10.34133/2022/9753506.
- (15) Richards, W. D.; Miara, L. J.; Wang, Y.; Kim, J. C.; Ceder, G. Interface Stability in Solid-State Batteries. *Chem. Mater.* **2016**, 28 (1), 266–273.
- (16) Woo, S.; Kang, B. Superior compatibilities of a LISICON-type oxide solid electrolyte enable high energy density all-solid-state batteries. *Journal of Materials Chemistry A* **2022**, *10* (43), 23185–23194.
- (17) Lu, J.; Li, Y. Perovskite-type Li-ion solid electrolytes: a review. *Journal of Materials Science: Materials in Electronics* **2021**, 32 (8), 9736–9754.
- (18) Xu, L.; Li, J.; Deng, W.; Shuai, H.; Li, S.; Xu, Z.; Li, J.; Hou, H.; Peng, H.; Zou, G.; Ji, X. Garnet Solid Electrolyte for Advanced All-Solid-State Li Batteries. *Adv. Energy Mater.* **2021**, *11* (2), 2000648.
- (19) Cheng, L.; Crumlin, E. J.; Chen, W.; Qiao, R.; Hou, H.; Franz Lux, S.; Zorba, V.; Russo, R.; Kostecki, R.; Liu, Z.; Persson, K.; Yang, W.; Cabana, J.; Richardson, T.; Chen, G.; Doeff, M. The origin of

- high electrolyte-electrode interfacial resistances in lithium cells containing garnet type solid electrolytes. *Phys. Chem. Chem. Phys.* **2014**, *16* (34), 18294–18300.
- (20) Xue, Z.; He, D.; Xie, X. Poly(ethylene oxide)-based electrolytes for lithium-ion batteries. *Journal of Materials Chemistry A* **2015**, 3 (38), 19218–19253.
- (21) Zheng, J.; Hu, Y.-Y. New Insights into the Compositional Dependence of Li-Ion Transport in Polymer–Ceramic Composite Electrolytes. ACS Appl. Mater. Interfaces 2018, 10 (4), 4113–4120.
- (22) Horowitz, Y.; Lifshitz, M.; Greenbaum, A.; Feldman, Y.; Greenbaum, S.; Sokolov, A. P.; Golodnitsky, D. Review—Polymer/Ceramic Interface Barriers: The Fundamental Challenge for Advancing Composite Solid Electrolytes for Li-Ion Batteries. *J. Electrochem. Soc.* 2020, 167 (16), 160514.
- (23) Lee, H.; Dellatore, S. M.; Miller, W. M.; Messersmith, P. B. Mussel-Inspired Surface Chemistry for Multifunctional Coatings. *Science* **2007**, *318* (5849), 426.
- (24) Ding, Y. H.; Floren, M.; Tan, W. Mussel-inspired polydopamine for bio-surface functionalization. *Biosurface and Biotribology* **2016**, 2 (4), 121–136.
- (25) Waite, J. H.; Tanzer, M. L. Polyphenolic Substance of Mytilus edulis: Novel Adhesive Containing L-Dopa and Hydroxyproline. *Science* **1981**, 212 (4498), 1038.
- (26) Wiegemann, M. Adhesion in blue mussels (Mytilus edulis) and barnacles (genus Balanus): Mechanisms and technical applications. *Aquatic Sciences* **2005**, *67* (2), 166–176.
- (27) Guo, L.; Liu, Q.; Li, G.; Shi, J.; Liu, J.; Wang, T.; Jiang, G. A mussel-inspired polydopamine coating as a versatile platform for the in situ synthesis of graphene-based nanocomposites. *Nanoscale* **2012**, 4 (19), 5864–5867.
- (28) Jia, M.; Zhao, N.; Bi, Z.; Fu, Z.; Xu, F.; Shi, C.; Guo, X. Polydopamine-Coated Garnet Particles Homogeneously Distributed in Poly(propylene carbonate) for the Conductive and Stable Membrane Electrolytes of Solid Lithium Batteries. *ACS Appl. Mater. Interfaces* **2020**, *12* (41), 46162–46169.
- (29) Ryou, M.-H.; Lee, D. J.; Lee, J.-N.; Lee, Y. M.; Park, J.-K.; Choi, J. W. Excellent Cycle Life of Lithium-Metal Anodes in Lithium-Ion Batteries with Mussel-Inspired Polydopamine-Coated Separators. *Adv. Energy Mater.* **2012**, *2* (6), 645–650.
- (30) Ryou, M.-H.; Lee, Y. M.; Park, J.-K.; Choi, J. W. Mussel-Inspired Polydopamine-Treated Polyethylene Separators for High-Power Li-Ion Batteries. *Adv. Mater.* **2011**, 23 (27), 3066–3070.
- (31) Kim, D. S.; Park, Y. J. A simple method for surface modification of carbon by polydopamine coating for enhanced Li–air batteries. *Electrochim. Acta* **2014**, *132*, 297–306.
- (32) Zhou, W.; Xiao, X.; Cai, M.; Yang, L. Polydopamine-Coated, Nitrogen-Doped, Hollow Carbon—Sulfur Double-Layered Core—Shell Structure for Improving Lithium—Sulfur Batteries. *Nano Lett.* **2014**, *14* (9), 5250—5256.
- (33) Jian, Z.; Li, H.; Cao, R.; Zhou, H.; Xu, H.; Zhao, G.; Xing, Y.; Zhang, S. Polydopamine-coated hierarchical tower-shaped carbon for high-performance lithium-sulfur batteries. *Electrochim. Acta* **2019**, *319*, 359–365.
- (34) Wang, S.-L.; Hong, J.-L. Polydopamine as an interfacial layer to enhance mechanical and adhesive properties of the active materials in a sulfur cathode of sodium-sulfur batteries. *Chemical Engineering Journal Advances* **2022**, *11*, No. 100352.
- (35) Yang, J.; Liu, G.; Avdeev, M.; Wan, H.; Han, F.; Shen, L.; Zou, Z.; Shi, S.; Hu, Y.-S.; Wang, C.; Yao, X. Ultrastable All-Solid-State Sodium Rechargeable Batteries. *ACS Energy Letters* **2020**, *5* (9), 2835–2841.
- (36) Liu, G.; Shi, J.; Zhu, M.; Weng, W.; Shen, L.; Yang, J.; Yao, X. Ultra-thin free-standing sulfide solid electrolyte film for cell-level high energy density all-solid-state lithium batteries. *Energy Storage Materials* **2021**, *38*, 249–254.
- (37) De Portu, G.; Babini, G. N. Mechanical Properties of Ceramics. In *Designing with Structural Ceramics*, Davidge, R. W., Van de Voorde, M. H., Eds.; Springer: Netherlands, 1991; pp 21–49 DOI: 10.1007/978-94-011-3678-5_2.

- (38) Lopez, J.; Pei, A.; Oh, J. Y.; Wang, G.-J. N.; Cui, Y.; Bao, Z. Effects of Polymer Coatings on Electrodeposited Lithium Metal. J. Am. Chem. Soc. 2018, 140 (37), 11735–11744.
- (39) Huang, Z.; Pang, W.; Liang, P.; Jin, Z.; Grundish, N.; Li, Y.; Wang, C.-A. A dopamine modified Li6.4La3Zr1.4Ta0.6O12/PEO solid-state electrolyte: enhanced thermal and electrochemical properties. *Journal of Materials Chemistry A* **2019**, *7* (27), 16425–16436.
- (40) Burfield, D. R.; Lee, K.-H.; Smithers, R. H. Desiccant efficiency in solvent drying. A reappraisal by application of a novel method for solvent water assay. *Journal of Organic Chemistry* **1977**, 42 (18), 3060–3065.
- (41) Burfield, D. R.; Smithers, R. H. Desiccant efficiency in solvent drying. 3. Dipolar aprotic solvents. *Journal of Organic Chemistry* **1978**, 43 (20), 3966–3968.
- (42) Wang, H.; Lin, C.; Zhang, X.; Lin, K.; Wang, X.; Shen, S. G. Mussel-Inspired Polydopamine Coating: A General Strategy To Enhance Osteogenic Differentiation and Osseointegration for Diverse Implants. ACS Appl. Mater. Interfaces 2019, 11 (7), 7615–7625.
- (43) Harvey, S.; Ng, D. Y. W.; Szelwicka, J.; Hueske, L.; Veith, L.; Raabe, M.; Lieberwirth, I.; Fytas, G.; Wunderlich, K.; Weil, T. Facile synthesis of ultrasmall polydopamine-polyethylene glycol nanoparticles for cellular delivery. *Biointerphases* **2018**, *13* (6), No. 06D407.
- (44) Cheng, E. J.; Kushida, Y.; Abe, T.; Kanamura, K. Degradation Mechanism of All-Solid-State Li-Metal Batteries Studied by Electrochemical Impedance Spectroscopy. *ACS Appl. Mater. Interfaces* **2022**, 14 (36), 40881–40889.
- (45) Krasnikova, I. V.; Pogosova, M. A.; Sanin, A. O.; Stevenson, K. J. Toward Standardization of Electrochemical Impedance Spectroscopy Studies of Li-Ion Conductive Ceramics. *Chem. Mater.* **2020**, 32 (6), 2232–2241.
- (46) Middlemiss, L. A.; Rennie, A. J. R.; Sayers, R.; West, A. R. Characterisation of batteries by electrochemical impedance spectroscopy. *Energy Reports* **2020**, *6*, 232–241.
- (47) Zhang, J.; Zhao, N.; Zhang, M.; Li, Y.; Chu, P. K.; Guo, X.; Di, Z.; Wang, X.; Li, H. Flexible and ion-conducting membrane electrolytes for solid-state lithium batteries: Dispersion of garnet nanoparticles in insulating polyethylene oxide. *Nano Energy* **2016**, 28, 447–454.
- (48) Larraz, G.; Orera, A.; Sanjuán, M. L. Cubic phases of garnet-type Li7La3Zr2O12: the role of hydration. *Journal of Materials Chemistry A* **2013**, *1* (37), 11419–11428.
- (49) Devaux, D.; Bouchet, R.; Glé, D.; Denoyel, R. Mechanism of ion transport in PEO/LiTFSI complexes: Effect of temperature, molecular weight and end groups. *Solid State Ionics* **2012**, 227, 119–127
- (50) Hoffman, Z. J.; Shah, D. B.; Balsara, N. P. Temperature and concentration dependence of the ionic transport properties of poly(ethylene oxide) electrolytes. *Solid State Ionics* **2021**, *370*, No. 115751.
- (51) Li, L.; Deng, Y.; Chen, G. Status and prospect of garnet/polymer solid composite electrolytes for all-solid-state lithium batteries. *Journal of Energy Chemistry* **2020**, *50*, 154–177.
- (52) Chen, L.; Li, Y.; Li, S.-P.; Fan, L.-Z.; Nan, C.-W.; Goodenough, J. B. PEO/garnet composite electrolytes for solid-state lithium batteries: From "ceramic-in-polymer" to "polymer-in-ceramic. *Nano Energy* **2018**, *46*, 176–184.
- (53) Sharafi, A.; Yu, S.; Naguib, M.; Lee, M.; Ma, C.; Meyer, H. M.; Nanda, J.; Chi, M.; Siegel, D. J.; Sakamoto, J. Impact of air exposure and surface chemistry on Li–Li7La3Zr2O12 interfacial resistance. *Journal of Materials Chemistry A* **2017**, *5* (26), 13475–13487.
- (54) Kaplan, W. D.; Chatain, D.; Wynblatt, P.; Carter, W. C. A review of wetting versus adsorption, complexions, and related phenomena: the rosetta stone of wetting. *J. Mater. Sci.* **2013**, 48 (17), 5681–5717.
- (55) Buschmann, H.; Dölle, J.; Berendts, S.; Kuhn, A.; Bottke, P.; Wilkening, M.; Heitjans, P.; Senyshyn, A.; Ehrenberg, H.; Lotnyk, A.; Duppel, V.; Kienle, L.; Janek, J. Structure and dynamics of the fast

- lithium ion conductor "Li7La3Zr2O12. Phys. Chem. Chem. Phys. 2011, 13 (43), 19378-19392.
- (56) Janani, N.; Deviannapoorani, C.; Dhivya, L.; Murugan, R. Influence of sintering additives on densification and Li+ conductivity of Al doped Li7La3Zr2O12 lithium garnet. *RSC Adv.* **2014**, *4* (93), 51228–51238.
- (57) Afyon, S.; Krumeich, F.; Rupp, J. L. M. A shortcut to garnet-type fast Li-ion conductors for all-solid state batteries. *Journal of Materials Chemistry A* **2015**, 3 (36), 18636–18648.
- (58) Botros, M.; Djenadic, R.; Clemens, O.; Möller, M.; Hahn, H. Field assisted sintering of fine-grained Li7–3xLa3Zr2AlxO12 solid electrolyte and the influence of the microstructure on the electrochemical performance. *J. Power Sources* **2016**, 309, 108–115.
- (59) Chan, C. K.; Yang, T.; Mark Weller, J. Nanostructured Garnet-type Li7La3Zr2O12: Synthesis, Properties, and Opportunities as Electrolytes for Li-ion Batteries. *Electrochim. Acta* **2017**, 253, 268–280
- (60) David, I. N.; Thompson, T.; Wolfenstine, J.; Allen, J. L.; Sakamoto, J. Microstructure and Li-Ion Conductivity of Hot-Pressed Cubic Li7La3Zr2O12. *J. Am. Ceram. Soc.* **2015**, 98 (4), 1209–1214.
- (61) Jang, J.; Oh, J.; Jeong, H.; Kang, W.; Jo, C. A Review of Functional Separators for Lithium Metal Battery Applications. *Materials* **2020**, *13* (20), 4625.
- (62) Belous, A. G.; V'yunov, O. I.; Kovalenko, L. L.; Bohnke, O.; Bohnke, C. Synthesis of thin-film electrodes based on LiPON and LiPON-LLTO-LiPON. Russian Journal of Electrochemistry **2014**, 50 (6), 523–530.
- (63) Dudney, N. J. Evolution of the lithium morphology from cycling of thin film solid state batteries. *Journal of Electroceramics* **2017**, 38 (2–4), 222–229.
- (64) Fu, K. K.; Gong, Y.; Dai, J.; Gong, A.; Han, X.; Yao, Y.; Wang, C.; Wang, Y.; Chen, Y.; Yan, C.; Li, Y.; Wachsman, E. D.; Hu, L. Flexible, solid-state, ion-conducting membrane with 3D garnet nanofiber networks for lithium batteries. *Proc. Natl. Acad. Sci. U. S. A.* 2016, 113 (26), 7094–7099.
- (65) Albertus, P.; Babinec, S.; Litzelman, S.; Newman, A. Status and challenges in enabling the lithium metal electrode for high-energy and low-cost rechargeable batteries. *Nature Energy* **2018**, *3* (1), 16–21.
- (66) Jiang, H.; Wu, Y.; Ma, J.; Liu, Y.; Wang, L.; Yao, X.; Xiang, H. Ultrathin polymer-in-ceramic and ceramic-in-polymer bilayer composite solid electrolyte membrane for high-voltage lithium metal batteries. *J. Membr. Sci.* **2021**, 640, No. 119840.